Journal Pre-proofs


Regular paper

# Performance Analysis of Power Beacon-Assisted Energy Harvesting NOMA Multi-user Relaying System over Nakagami-*m* Fading Channels

Tran Manh Hoang, Nguyen Trung Tan, Xuan Nam Tran, Le The Dung

PII: S1434-8411(19)32156-9
DOI: https://doi.org/10.1016/j.aeue.2019.153022
Reference: AEUE 153022

To appear in: *International Journal of Electronics and Communications*

Received Date: 27 August 2019
Accepted Date: 29 November 2019

Please cite this article as: T.M. Hoang, N.T. Tan, X.N. Tran, L.T. Dung, Performance Analysis of Power Beacon-Assisted Energy Harvesting NOMA Multi-user Relaying System over Nakagami-*m* Fading Channels, *International Journal of Electronics and Communications* (2019), doi: https://doi.org/10.1016/j.aeue.2019.153022

# Performance Analysis of Power Beacon-Assisted Energy Harvesting NOMA Multi-user Relaying System over Nakagami-$m$ Fading Channels

Tran Manh Hoang[a,b], Nguyen Trung Tan[b], Xuan Nam Tran[b], Le The Dung[c,d,*]

[a] *Faculty of Telecommunications Services, Telecommunications University, Vietnam*
[b] *Faculty of Radio Electronics, Le Quy Don Technical University, Vietnam*
[c] *Divison of Computational Physics, Institute for Computational Science, Ton Duc Thang University, Ho Chi Minh City, Vietnam*
[d] *Faculty of Electrical and Electronics Engineering, Ton Duc Thang University, Ho Chi Minh City, Vietnam*

**Abstract**

In this paper, we propose and analyze a multi-user non-orthogonal multiple access (NOMA) relaying system under the effect of Nakagami-$m$ fading. In this system, both source and the relay harvest the energy from a multiple-antenna power beacon (PB) in the first time duration by using the time switching protocol and then use the harvested energy to transmit and receive the signals in the remaining time duration. We derive the exact closed-form expressions of the outage probability in two cases of successive interference cancellation (SIC), i.e. perfect SIC and imperfect SIC. Moreover, we determine the optimal time swiching ratio that maximizes the system throughput. We also compare the achievable sum rate of the proposed NOMA relaying system with that of the orthogonal multiple access (OMA) relaying system. The correctness of all derived mathematical expressions results in this paper is verified by Monte-Carlo simulations. Numerical results show that: 1) the fading severity of wireless channels has a significant impact on the outage probability and the diversity; 2) increasing the number of antennas of PB helps to lower the outage probability, decrease the energy harvesting time, and increase the throughput; 3) the sum rate of the proposed NOMA relaying system is proportional with the SIC quality and is higher than that of the OMA relaying system in low and moderate (SNR) regimes.

*Keywords:* non-orthogonal multiple access, power beacon, energy harvesting, successive interference cancellation, performance evaluation

## 1. Introduction

Nowadays, the Internet of Things (IoT) has received increasing attentions from both industry and academy. It is considered as an important mean for wireless connections in the era of the fourth industry. IoT has been employed in the advanced wireless standards such as the fourth generation (4G) and is currently being considered for the fifth generation (5G) of mobile communications. To support the operations of large multi-user systems such as IoT, the non-orthogonal multiple access (NOMA) is very potential due to its high bandwidth efficiency [1, 2]. Moreover, compared with conventional multiple access systems such as time-division multiple access (TDMA), code-division multiple access (CDMA), orthogonal frequency-division multiple access (OFDMA), NOMA systems offer better fairness among users, even for users with weak CSI.

*Corresponding author
*Email address:* lethedung@tdtu.edu.vn (Le The Dung )

To deal with the massive connectivity and low latency in IoT, the authors of [3] introduced a new millimeter-wave (mmWave)-NOMA transmission scheme designed for cellular machine-to-machine (M2M) communication systems for IoT applications. It was demonstrated that the proposed cellular M2M communication system using the mmWave-NOMA transmission scheme improves outage probability compared with equivalent systems using mmWave with orthogonal multiple access (OMA) scheme. Meanwhile, combining NOMA with the simultaneous wireless information and power transfer (SWIPT) helps to prolong the network lifetime and improve the spectral utilizing efficiency of NOMA systems [4–6]. Another study of the energy efficiency in NOMA system was presented in [7]. The authors used the fractional programming to solve the power optimization problem so that the energy efficiency can be maximized. The authors of [8] examined the system, in which near NOMA users closing to the source act as energy harvesting relays to help far NOMA users. Three user selection schemes based on the user distances form the base station were proposed to achieve low outage probability and deliver superior throughput in comparison to the random selection scheme. In [9], a dual-hop communication in an ambient RF energy harvesting NOMA system, where a source wants to transmit simultaneously symbols to two desired destinations via relay, was analyzed. The impact of power allocation in cooperative NOMA system with SWIPT was studied in [10]. The authors investigate the impact of two types of proposed NOMA power allocation policies, namely NOMA with fixed power allocation (F-NOMA) and cognitive radio inspired NOMA (CR-NOMA). It was shown that these proposed NOMA schemes can effectively reduce the outage probability compared with the conventional SWIP relaying network.

Unfortunately, due to a big gap between the active sensitivity of the energy harvester and that of the decoder, i.e. -10 dBm and -60 dBm, SWIPT-based systems are only appropriate for short-distance communication. To overcome this limitation, power beacon (PB) is used to supply power for wireless devices. The advantage of PB-assited SWIPT is fully controllable, thus it can provide various applications with high quality of service (QoS) requirements. Specifically, three wireless power transfer models, namely, cooperative PBs power transfer, best PB power transfer, and nearest PBs power transfer were introduced in [11] to enable wireless energy harvesting and secure information transmission in energy harvesting large-scale cognitive cellular networks. The authors of [12] concern about enabling microwave power transfer for mobile recharging in cellular networks. They proposed a new network architecture that overlays an uplink cellular network with random deployed PBs for powering mobiles, called a hybrid network. In [13], the authors studied the outage performance of multihop cognitive relay networks with energy harvesting in underlay paradigms, wherein the transmission of secondary user is subject to the harvested energy from PB and the interference constraint. The optimization problems of energy allocation and time splitting for PB-assisted SWIPT networks was considered in [14, 15]. Unlike aforementioned works which used linear EH model, [16–18] investigated NOMA systems with more practical EH model, i.e. the non-linear EH model. Specifically, assuming two practical non-linear EH models, a robust resource optimization problem is studied in [16]. The proposed algorithm can achieve a good tradeoff between the consumed power and the harvested power in a multiple-input single output (MISO) cognitive radio network with SWIPT under imperfect CSI. In [17], a minimum transmission power problem is formulated under the non-linear EH model and bounded CSI error in a NOMA MISO cognitive network. The authors jointly designed the beamforming weights and the power splitting ratio for minimizing the transmission power of the cognitive base station. This work was extended in [18] by

proposing an artificial-noise-aided cooperative jamming scheme to improve the security of primary network.

Although the fundamentals of NOMA and energy harvesting (EH) have been investigated in the literature, so far there is a lack of study on NOMA relaying systems where the energy is harvested from PB. In the aforementioned works, only point-to-point EH communication systems were considered and the operating frequency of PB is different from that of the information transceiver. Additionally, the successive interference cancellation (SIC) has often assumed to be perfect. Regarding to the wireless channel model, it is well-known that Nakagami-$m$ is a generic distribution whose value of $m$ can be adjusted to model a variety of wireless channels such as Rayleigh and Rician fading channels. However, it is extremely challenging to derive the mathematical expressions for the analysis of EH-NOMA systems over Nakagami-$m$ fading channels due to the calculation complexity. Motivated by these observations, in this paper, we mathematically analyze in detail a PB-assisted EH-NOMA multi-user relaying system over Nakagami-$m$ fading channels. The main objective of this work is to understand the fundamental limit of wireless powered in NOMA communication and characterize the impact of key system parameters on the OP, sum rate of NOMA relaying system. In particular, we analyze the OP under two cases, i.e. perfect SIC and imperfect SIC. Moreover, we study the scenario where the energy is transmitted from PB, which has not been considered in the literature. The advantage of PB assisted EH is easily controlled, stable amount of energy. Therefore it can be applied in healthcare and medical networks with low-power medical devices.

The contributions of this paper can be summarized as follows:

- Contrary to the previous works [19, 20] which studied the NOMA systems with fixed power supply and perfect SIC, we propose a NOMA system where both source and relay harvest the RF energy from a multiple-antenna PB and use the harvested energy to transmit and receive data. Moreover, PB only transmits energy during the energy harvesting phase of source and relay to save the energy.

- We analyze the performance of the proposed PB-assisted EH-NOMA multi-user relaying system for the cases of perfect and imperfect SIC over Nakagami-$m$ fading channel, which is a generic fading channel. Therefore, the performance of this NOMA relaying system over Rayleigh and Rician fading channels can be obtained by modifying the Nakagami-$m$ fading channel. More specifically, we derive the exact mathematical expression of the outage probability of each user for both perfect and imperfect SIC. Then, we determine the optimal time switching ratio for the energy transmission and reception among PB, source, and relay so that the instantaneous throughput of the system can be maximized. Finally, the sum rate of the considered NOMA relaying system is also compared with that of the OMA relaying system.

- We present various Monte-Carlo simulation results to corroborate our analysis and show the influences of the fading severity of wireless channels, the number of antennas of PB, and the SIC quality on the outage probability, throughput, and sum rate of the proposed NOMA relaying system in comparison with OMA relaying system.

The rest of this paper is organized as follows. Section 2 describes the system model of the proposed PB-assisted EH-NOMA multi-user relaying system. The mathematical analysis of the outage probability of the considered NOMA relaying system for perfect and imperfect SIC, the calculation of optimal time switching ratio, and the

comparison of the sum rates of NOMA and OMA relaying systems are presented in Section 3. Numerical results are given in Section 4. Finally, Section 5 concludes the paper.

For the convenience, we provide in Table 1 the mathematical notations along with their descriptions used in this paper.

Table 1: The mathematical notations used in this paper.

| Notation | Description |
|---|---|
| $N$ | The number of users |
| $K$ | The number of antennas of the power beacon |
| $a_n$ | Power allocation coefficient |
| $d_n$ | The distance between R and $\mathrm{D}_n$ |
| $r_n$ | The threshold data rate of $\mathrm{D}_n$ |
| $f_1, f_2, h_1, g_n$ | The channel coefficients of $\mathrm{PB}-\mathrm{S}$, $\mathrm{PB}-\mathrm{R}$, $\mathrm{S}-\mathrm{R}$, and $\mathrm{R}-\mathrm{D_n}$ channels |
| $\mathbb{E}\{\cdot\}$ | Expectation operator |
| $\Gamma(\cdot)$ | Gamma function [21] |
| $\mathcal{K}_n(\cdot)$ | $n$th order Bessel function of the second kind [21] |
| $\mathrm{E}_n(z)$ | Exponential integral function [21] |
| $G_{pq}^{mn}(x\|_{b_s}^{a_r})$ | Meijer's G-function [21, Sect. 9.3] |
| $W(z)$ | Lambert function |
| $\|\cdot\|$ | Frobenius norm |
| $\dagger$ | Conjugate transpose operator |
| $\alpha$ | Time switching ratio |
| $\eta$ | Energy conversion efficiency |
| $\delta_1, \delta_2$ | The levels of residual interference at R and $\mathrm{D}_n$ |
| $m_{\mathrm{PS}}$, $m_{\mathrm{PR}}$, $m_{\mathrm{SR}}$, $m_{\mathrm{RD}_n}$ | The fading severity of $\mathrm{PB}-S$, $\mathrm{PB}-R$, $\mathrm{S}-\mathrm{R}$, and $\mathrm{R}-\mathrm{D}_n$ channels |
| $w_{\mathrm{S}}, w_{\mathrm{R}}, w_{\mathrm{D}_n}$ | The additive white Gaussian noise (AWGN) at S, R, and $\mathrm{D}_n$ |

## 2. System model

The system model considered in this paper is a downlink multi-user NOMA relaying system. It consists of a source (S) communicating simultaneously with $N$ users ($\mathrm{D}_n$, $n \in \{1, \cdots, N\}$) via a relay (R) by using decode-and-forward protocol [22]. Similar to [23], $\mathrm{D}_n$ is powered by a fixed power supply such as batteries. Meanwhile, S and R have limited power supply, thus they need to harvest the energy from a multiple-antenna PB. In other words, the PB serves as the energy source to support the signal transmission of S and the signal reception of R. The PB is located in a convenient location such that the $\mathrm{PB}-\mathrm{S}$ and $\mathrm{PB}-\mathrm{R}$ links are available. Moreover, it can do channel estimation, spectrum sensing, and digital beamforming.

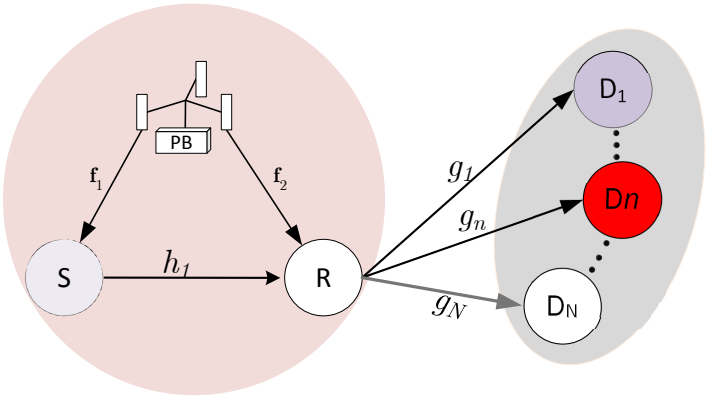


Figure 1: System model of the proposed PB-assisted EH-NOMA multi-user relaying system.

All nodes S, R, and $D_n$ have single antennas and operate in half duplex mode. The direct link between S and $D_n$ is not available due to the long distance between them. The PB−S, PB−R, S − R, and R − $D_n$ channels are modeled by Nakagami-$m$ fading distributions [24, pp. 200] with $f_1 \sim \mathcal{G}(m_{\rm PS}, \frac{m_{\rm PS}}{\Omega_{\rm PS}})$, $f_2 \sim \mathcal{G}(m_{\rm PR}, \frac{m_{\rm PR}}{\Omega_{\rm PR}})$, and $h_1 \sim \mathcal{G}(m_{\rm SR}, \frac{m_{\rm SR}}{\Omega_{\rm SR}})$ respectively refer to their complex channel coefficients, where $\Omega_{\rm PS} = \mathbb{E}\{|f_1|^2\}$, $\Omega_{\rm PR} = \mathbb{E}\{|f_2|^2\}$, $\Omega_{\rm SR} = \mathbb{E}\{|h_1|^2\}$. Additionally, perfect time synchronization among S, R, and PB happens at the initial state of the first time slot.

We denote $\sqrt{d_n^{-\beta}}$ and $\tilde{g}_n$ as the large-scale fading and small-scale fading coefficients of S − R and R − $D_n$ channels, where $d_n$ are the distances between S and R, and between R and $D_n$, $\beta$ is the path loss factor. Then, $g_n = \tilde{g}_n\sqrt{d_n^{-\beta}}$ follows Nakagami distribution with mean $m_{{\rm RD}_n}$ and variance $\frac{m_{{\rm RD}_n}}{\Omega_{{\rm RD}_n}}$, i.e. $g_n \sim \mathcal{G}(m_{{\rm RD}_n}, \frac{m_{{\rm RD}_n}}{\Omega_{{\rm RD}_n}})$, where $\Omega_{{\rm RD}_n} = \mathbb{E}\{|g_n|^2\}$. Since all channel coefficients follow i.n.i.d Nakagami-$m$ distributions, the channel gains are characterized by Gamma distributions. Without loss of generality, we assume that $d_1 > d_2, \cdots, > d_N$. Then, the channel gains are sorted according to an ascending order $|g_1|^2 <, \cdots, < |g_N|^2$.

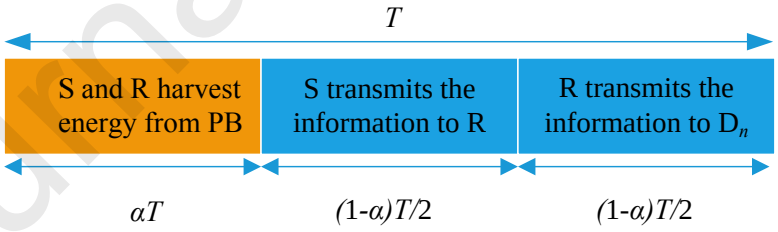


Figure 2: The operation of the proposed PB-assisted EH-NOMA multi-user relaying system.

When harvesting the energy, S and R use the time switching (TS) protocol with $T$ represents the transmission block period from S to $D_n$ as depicted in Fig. 2. During each period $T$, the first time duration $\alpha T$, where $\alpha$ is the time-switching ratio and $0 \leq \alpha < 1$, is used for S and R to harvest the RF energy from PB. The remaining time duration $(1-\alpha)T$ is used for transmitting and forwarding data from S to $D_n$. It should be noted that, when $\alpha = 1$ (the energy harvesting time duration takes total block time), S and R do not process any signals. As a result, the basic role in signal forwarding of R is eliminated [25]. Therefore, we do not consider this case.

## 3. Performance analysis

In this section, we mathematically investigate the outage probability and determine the optimal time switching ratio of the proposed PB-assisted EH-NOMA multi-user relaying system. Then, we compare the sum rates of NOMA and OMA relaying systems.

Firstly, the principles of the system operation are presented as follows. Since PB is equipped with $K$ antennas to improve the efficiency of energy transfer, the maximal ratio transmission (MRT) scheme is applied. Thus, the signal vector $\mathbf{x}_s$ with a size of $K \times 1$ transmitted by PB is given by

$$\mathbf{x}_s = \mathbf{w}_\ell s_e, \tag{1}$$

where $\mathbf{w}_\ell = \mathbf{f}_\ell^\dagger / \|\mathbf{f}_\ell\|$, $\ell \in \{1, 2\}$ and $\|\mathbf{w}_\ell\|^2 = 1$, refers to the beamforming vectors from PB to S and R; $s_e$ is the energy symbol with unit power.

To optimize the beamforming vector $\mathbf{w}_\ell$, the elements $\mathbf{f}_\ell = [f_{\ell,1}, \cdots, f_{\ell,K}]$ designed at PB are assumed to be independent and identically distributed (i.i.d.). During the energy harvesting phase, the energy signal received at S and R are respectively expressed as [14, 26]

$$\begin{aligned} y_{\mathrm{S}} &= \sqrt{P_{\mathrm{PB}}}\mathbf{f_1}\mathbf{x}_s + w_{\mathrm{S}}, \\ y_{\mathrm{R}} &= \sqrt{P_{\mathrm{PB}}}\mathbf{f_2}\mathbf{x}_s + w_{\mathrm{R}}, \end{aligned} \tag{2}$$

where $w_{\mathrm{S}}$ and $w_{\mathrm{R}}$ are the additive white Gaussian noises (AWGNs) at S and R, respectively. They can be modeled as $w_{\mathcal{A}} \sim \mathcal{CN}(0, \sigma_{\mathcal{A}}^2)$, where $\mathcal{A} \in \{\mathrm{S}, \mathrm{R}\}$ and $\sigma_{\mathcal{A}}^2 = \mathbb{E}\{w_{\mathcal{A}} w_{\mathcal{A}}^*\}$ is the noise variance at the energy receivers [14].

We should remind that converting the signal from RF band to the baseband does not need to perform at the EH circuit because the purpose is to harvest the carried energy. Thus, the background noise of the EH receiver is not considered. However, the analysis framework in this paper can be extended for the cases when background noise and co-channel interference impact the performance of EH systems.

Then, the amounts of energy harvested at S and R in the case of perfect CSI at the end of the energy harvesting phase are respectively given by [25, 27]

$$E_{\mathrm{S}} = \eta\alpha T P_{\mathrm{PB}} ||\mathbf{f_1}||^2, \tag{3}$$

$$E_{\mathrm{R}} = \eta\alpha T P_{\mathrm{PB}} ||\mathbf{f_2}||^2, \tag{4}$$

where $\eta$, $0 < \eta < 1$, is the energy conversion efficiency coefficient, $P_{\mathrm{PB}}$ is the transmission power of PB.

Since the harvest-use (HU) energy harvesting architecture is used[1], S and R do not need batteries to store the harvested energy. Instead, they consume all harvested energy immediately. Therefore, from (3) and (4), the transmission power of S and R are respectively expressed as

$$P_{\mathrm{S}} = \frac{E_{\mathrm{S}}}{(1-\alpha)T/2} = \frac{2\eta\alpha P_{\mathrm{PB}} ||\mathbf{f_1}||^2}{(1-\alpha)}, \tag{5}$$

$$P_{\mathrm{R}} = \frac{E_{\mathrm{R}}}{(1-\alpha)T/2} = \frac{2\eta\alpha P_{\mathrm{PB}} ||\mathbf{f_2}||^2}{(1-\alpha)}. \tag{6}$$

[1]In the case that harvest-use-store (HUS) energy harvesting architecture is used, the total energy of S or R at any time slot is $E_{\mathcal{A}} = \eta\alpha T P_{\mathrm{PB}} ||\mathbf{f}_\ell||^2 + E_0$, where $E_0$ is the residual energy.

As aforementioned, since the channel coefficients $h_1$ and $g_n$ follow Nakagami-$m$ distributions, $|h_1|^2$, $|g_n|^2$ are modeled by Gamma distributions [24, 28], whose cumulative distribution function (CDF) and probability density function (PDF) are given by

$$F_{\mathcal{X}}(x) = 1 - \exp\left(-\frac{mx}{\Omega_{\mathcal{A}}}\right) \sum_{k=1}^{m-1} \frac{1}{k!} \left(\frac{mx}{\Omega_{\mathcal{A}}}\right)^k, \tag{7}$$

$$f_{\mathcal{X}}(x) = \left(\frac{m}{\Omega_{\mathcal{A}}}\right)^m \frac{x^{m-1}}{\Gamma(m)} \exp\left(-\frac{mx}{\Omega_{\mathcal{A}}}\right), \tag{8}$$

where random variable $\mathcal{X} \in \{|h_1|^2, |g_n|^2\}$ and $\Gamma(\cdot)$ is the Gamma function with $m = \frac{\mathbb{E}^2\{\mathcal{X}\}}{var\{\mathcal{X}\}}$ is the inverse of the normalized variance of $\mathcal{X}$.

The PB−S and PB−R channels are modeled by Nakagami-$m$ distributions with independent and identically distributed elements $\mathbf{f}_\ell = [f_{\ell,1}, \cdots, f_{\ell,K}]$. Hence, the CDF and PDF of $||\mathbf{f}_\ell||^2$ are respectively given by

$$F_{||\mathbf{f}_\ell||^2}(y) = 1 - \exp\left(-\frac{m_\ell y}{\Omega_\ell}\right) \sum_{\nu=0}^{Km_\ell-1} \frac{1}{\nu!} \left(\frac{m_\ell y}{\Omega_\ell}\right)^\nu, \tag{9}$$

$$f_{||\mathbf{f}_\ell||^2}(y) = \left(\frac{m_\ell}{\Omega_\ell}\right)^{Km_\ell} \frac{y^{Km_\ell-1}}{\Gamma(Km_\ell)} \exp\left(-\frac{m_\ell y}{\Omega_\ell}\right), \tag{10}$$

where $m_\ell$ is the fading parameter.

Based on the above properties of the system model, its performance will be mathematically analyzed in the following subsections.

### *3.1. Outage probability with perfect SIC*

In this subsection, we derive the outage probability of $\mathrm{D}_n$. For the fairness among users, the required data rate from S to $\mathrm{D}_n$ is considered as not similar due to the differences in channel gains. Moreover, since S transmits the superimposed signals, $x_{\mathrm{S}} = \sum_{n=1}^{N} \sqrt{a_n P_S} x_n$, where $a_n$ denotes the power allocation coefficient for the $n$th signal such that $\sum_{n=1}^{N} \sqrt{a_n} = 1$.

According to the TS protocol, the communicating operation of the system over time duration $(1-\alpha)T$ is divided into two communication phases. In the first communication phase, the received signal at R is given by

$$y_{\mathrm{R}} = \sqrt{\frac{2\eta\alpha P_{\mathrm{PB}} ||\mathbf{f_1}||^2}{1-\alpha}} h_1 \sum_{n=1}^{N} \sqrt{a_n} x_n + w_{\mathrm{R}}. \tag{11}$$

By using DF protocol, R first decodes the symbols by applying the successive interference cancellation (SIC), then re-encodes with the superposed signals, and finally forwards them to $\mathrm{D}_n$. To decode the $n$th signal, R needs to perform SIC to cancel the signals of other users. In addition, to increase the efficiency of SIC, R decodes the signal having higher power level while treating the remaining signals as noises. Thus, the instantaneous signal-to-interference-noise ratio (SINR) of $\mathrm{S} - \mathrm{R}$ link is

$$\Gamma_1^n = \frac{a_n \phi \|\mathbf{f_1}\|^2 |h_1|^2}{\sum_{i=n+1}^{N} a_i \phi ||\mathbf{f_1}||^2 |h_1|^2 + \sigma_{\mathrm{R}}^2}, \tag{12}$$

where $\phi = \frac{2\alpha\eta P_{\mathrm{PB}}}{1-\alpha}$.

In the second communication phase, the received signal at $\mathrm{D}_n$ is given by

$$y_{\mathrm{D}_n} = \sqrt{\frac{2\eta\alpha P_{\mathrm{PB}}||\mathbf{f_2}||^2}{1-\alpha}} g_n \sum_{n=1}^{N} \sqrt{a_n} x_n + w_{\mathrm{D}_n}. \tag{13}$$

From (13), the SINR of $\mathrm{D}_n$ when the signal of $j$th user, $j < n$, exists is expressed as

$$\Gamma_2^{j\to n} = \frac{a_j \phi ||\mathbf{f_2}||^2 |g_n|^2}{\sum_{i=j+1}^{N} a_i \phi ||\mathbf{f_2}||^2 |g_n|^2 + \sigma_{\mathrm{D}_n}^2}. \tag{14}$$

Then, $\mathrm{D}_n$ performs SIC until its symbols are detected successfully. Consequently, the SINR of $\mathrm{D}_n$ is

$$\Gamma_2^{n} = \frac{a_n \phi ||\mathbf{f_2}||^2 |g_n|^2}{\sum_{i=n+1}^{N} a_i \phi ||\mathbf{f_2}||^2 |g_n|^2 + \sigma_{\mathrm{D}_n}^2}. \tag{15}$$

Since the relay node uses DF protocol, the dual-hop path can be modeled as an equivalent single-hop path [29] whose output SNR can be tightly approximated as $\Gamma_{e2e} = \min(\Gamma_1^n, \Gamma_2^{j\to n})$ in the high SNR regime. Let us define $\mathrm{OP} = \Pr(\Gamma_{e2e} < \gamma_{\mathrm{th}})$ as the probability that the outage event occurs in the system, where $\gamma_{\mathrm{th}} = 2^{2r_n/(1-\alpha)} - 1$ is the predefined threshold of the SINR to ensure quality-of-service (QoS), $r_n$ is the threshold data rate of $\mathrm{D}_n$.

Define $\Lambda_1^{n,j} < \gamma_{\mathrm{th}_j}$ as the outage event that R cannot decode the signal of $\mathrm{D}_j$, i.e. the SINR of the signal for $\mathrm{D}_j$ falls below threshold $\gamma_{\mathrm{th}_j}$ at R, and $\Lambda_2^{n,j} < \gamma_{\mathrm{th}_j}$ as the outage event that $\mathrm{D}_n$ cannot decode its own signal or the signal of $j$th user, $1 \le j \le n$. Then, the OP of $\mathrm{D}_n$ can be calculated as

$$\mathrm{OP}_n = 1 - \Pr(\Lambda_1^{n,1} \cap \cdots \cap \Lambda_1^{n,n}) \Pr(\Lambda_2^{n,1} \cap \cdots \cap \Lambda_2^{n,n}). \tag{16}$$

When $j = N$, it corresponds to the case that SIC will be implemented until all signals of the last user $D_N$ are decoded. Without loss of generality, we assume that the variance of AWGN $\sigma_{\mathrm{R}}^2 = \sigma_{\mathrm{D}_N}^2 = 1$, and SIC is perfect. Thus, the SNR at $\mathrm{D}_N$ is given by $a_N \phi \|\mathbf{f_1}\|^2 |h_1|^2 > \gamma_{\mathrm{th}_N}$ and $a_N \phi ||\mathbf{f_2}||^2 |g_N|^2 > \gamma_{\mathrm{th}_N}$.

When, $j \neq N$, by defining $\theta_n^* = \max[\gamma_{\mathrm{th}_1}, \gamma_{\mathrm{th}_2}, \cdots, \gamma_{\mathrm{th}_n}]$, the outage probability of the $n$th user can be reformulated as

$$\mathrm{OP}_n = 1 - \underbrace{\Pr(\Gamma_1^n > \theta_n^*)}_{\mathcal{O}_1} \underbrace{\Pr(\Gamma_2^{j\to n} > \theta_n^*)}_{\mathcal{O}_2}. \tag{17}$$

After some manipulations, we have the closed-form expression of the OP of $\mathrm{D}_n$ as

$$\begin{aligned}\mathrm{OP}_n = 1 - & \sum_{\nu=0}^{Km_1-1} \frac{2}{\nu!\Gamma(m_{\mathrm{SR}})} \left(\frac{m_1\chi_1}{\Omega_{\mathrm{PS}}}\right)^{\nu} \left(\frac{m_1\Omega_{\mathrm{SR}}\chi_1}{m_{\mathrm{SR}}\Omega_{\mathrm{PS}}}\right)^{\frac{m_{\mathrm{SR}}-\nu}{2}} \left(\frac{m_{\mathrm{SR}}}{\Omega_{\mathrm{SR}}}\right)^{m_{\mathrm{SR}}} \mathcal{K}_{m_{\mathrm{SR}}-\nu}\left(2\sqrt{\frac{m_1 m_2 \chi_1}{\Omega_{\mathrm{PS}}\Omega_{\mathrm{SR}}}}\right) \\ & \times \sum_{t=0}^{N-1} \sum_{n=0}^{Km_2-1} \sum_{k=0}^{t(m_{\mathrm{RD}_n}-1)} \frac{1}{k!} \binom{N-1}{t} \frac{N(-1)^t b_k^t}{\Gamma(m_{\mathrm{RD}_n})^{N-1}} \left(\frac{m_{\mathrm{RD}_n}}{\Omega_{\mathrm{RD}_n}}\right)^{m_{\mathrm{RD}_n}+k} \left(\frac{m_2\chi_2}{\Omega_{\mathrm{PR}}}\right)^{n} \\ & \times 2\left(\frac{m_2\Omega_{\mathrm{RD}_n}\chi_2}{m_{\mathrm{RD}_n}(t+1)\Omega_{\mathrm{PR}}}\right)^{\frac{k+m_{\mathrm{RD}_n}-n}{2}} \mathcal{K}_{k+m_{\mathrm{RD}_n}-n}\left(2\sqrt{\frac{m_2 m_{\mathrm{RD}_n}(t+1)\chi_2}{\Omega_{\mathrm{PS}}\Omega_{\mathrm{SR}}}}\right),\end{aligned} \tag{18}$$

where $\chi_1 = \frac{\theta_n^*}{\phi(a_n - \theta_n^* \sum_{i=n+1}^{N} a_i)}$, $\chi_2 = \frac{\theta^*}{\phi(a_n - \theta^* \sum_{i=j+1}^{N} a_i)}$, $\mathcal{K}_u(\cdot)$ is the $u$th order modified Bessel function of the

second kind [21, Eq. (8.407.1)], and the coefficient $b_k^t$ can be recursively calculated as [21, Eq. (0.314)]

$$b_0^t = 1, b_1^t = t, b_{t(m_{\mathrm{RD}_n}-1)}^t = \left(\frac{1}{(m_{\mathrm{RD}_n}-1)!}\right)^t \tag{19a}$$

$$b_k^t = \frac{1}{k}\sum_{j=1}^{J_0}\frac{j\,(t+1)-k}{j!}b_{k-j}^t \tag{19b}$$

$$J_0 = \min\left(k,\, m_{\mathrm{RD}_n}-1\right), \quad 2 \le k \le t\,(m_{\mathrm{RD}_n}-1)-1, \tag{19c}$$

We should note that the condition $a_n > \theta^* \sum_{i=n+1}^{N} a_i$ helps to ensure that $\chi_1$ is always positive, i.e. the allocated power for $\mathrm{D}_n$ is higher than the others. Otherwise, the outage always occurs.

### *3.2. Outage probability with imperfect SIC*

In practice, it is very difficult to achieve an ideal SIC structure. The imperfect SIC, which is caused by the hardware limitation of the receiver, is one of the reasons of the error propagation when decoding the signals of NOMA users. Hence, investigating the effect of imperfect SIC is necessary when designing NOMA network, which will be presented in this subsection.

Generally, there exits the residual power at $\mathrm{D}_n$ user due to the imperfect removal of other users signals. Therefore, the signal of $\mathrm{D}_n$ at the output of SIC structure of R in the first phase can be expressed as

$$y_{\mathrm{R}} = \underbrace{h_1\sqrt{a_n\frac{2\eta\alpha P_{\mathrm{PB}}||\mathbf{f_1}||^2}{(1-\alpha)}}x_n}_{\text{signal of } n\text{th user}} + \underbrace{h_1\sum_{i=n+1}^{N}\sqrt{a_i\frac{2\eta\alpha P_{\mathrm{PB}}||\mathbf{f_1}||^2}{(1-\alpha)}}x_i}_{\text{signal of other users}} + \underbrace{h_1\sum_{j=1}^{n-1}\sqrt{\delta_1 a_j\frac{2\eta\alpha P_{\mathrm{PB}}||\mathbf{f_1}||^2}{(1-\alpha)}}x_j}_{\text{imperfect SIC}} + w_{\mathrm{R}}, \tag{20}$$

where $j < i \le n \le N$.

At the end of the second phase, the signal at the output of SIC structure of $\mathrm{D}_n$ is

$$y_{\mathrm{D}_n} = \underbrace{g_n\sqrt{a_n\frac{2\eta\alpha P_{\mathrm{PB}}||\mathbf{f_2}||^2}{(1-\alpha)}}x_n}_{\text{signal of } n\text{th user}} + \underbrace{g_n\sum_{i=n+1}^{N}\sqrt{a_i\frac{2\eta\alpha P_{\mathrm{PB}}||\mathbf{f_2}||^2}{(1-\alpha)}}x_i}_{\text{signals of other users}} + \underbrace{g_n\sum_{j=1}^{n-1}\sqrt{\delta_2 a_j\frac{2\eta\alpha P_{\mathrm{PB}}||\mathbf{f_2}||^2}{(1-\alpha)}}x_j}_{\text{imperfect SIC}} + w_{\mathrm{D}_n}, \tag{21}$$

where $\delta_1$ and $\delta_2$ represent the impact levels of the residual interference at the output of SIC structure of R and $\mathrm{D}_n$, respectively.

From (20) and (21), we have the instantaneous SINRs at R and $\mathrm{D}_n$ as follows

$$\Gamma_{1,n}^{impSIC} = \frac{a_n\phi||\mathbf{f_1}||^2|h_1|^2}{\sum_{i=n+1}^{N}a_i\phi||\mathbf{f_1}||^2|h_1|^2 + \delta_1\sum_{j=1}^{n-1}a_j\phi||\mathbf{f_1}||^2|h_1|^2 + \sigma_{\mathrm{R}}^2}, \tag{22}$$

$$\Gamma_{2,n}^{impSIC} = \frac{a_n\phi||\mathbf{f_2}||^2|g_n|^2}{\sum_{i=n+1}^{N}a_i\phi||\mathbf{f_2}||^2|g_n|^2 + \delta_2\sum_{j=1}^{n-1}a_j\phi||\mathbf{f_2}||^2|g_n|^2 + \sigma_{\mathrm{D}_n}^2}. \tag{23}$$

Similar to Section 3.1, the OP in the case of imperfect SIC can be calculated as

$$\mathrm{OP}_n^{impSIC} = 1 - \Pr(\Gamma_{1,n}^{impSIC} > \theta_n^*)\Pr(\Gamma_{2,n}^{impSIC} > \theta_n^*). \tag{24}$$

Plugging (22) and (23) into (24), we obtain the OP in the case of imperfect SIC as

$$\begin{aligned}\mathrm{OP}_n^{impSIC} = 1- &\sum_{k=0}^{Km_1-1} \frac{2}{k!\Gamma(m_{\mathrm{SR}})}\left(\frac{m_1\Delta_1}{\Omega_{\mathrm{PS}}}\right)^k\left(\frac{m_1\Omega_{\mathrm{SR}}\Delta_1}{m_{\mathrm{SR}}\Omega_{\mathrm{PS}}}\right)^{\frac{m_{\mathrm{SR}}-k}{2}}\left(\frac{m_{\mathrm{SR}}}{\Omega_{\mathrm{SR}}}\right)^{m_{\mathrm{SR}}}\mathcal{K}_{m_{\mathrm{SR}}-k}\left(2\sqrt{\frac{m_1m_2\Delta_1}{\Omega_{\mathrm{PS}}\Omega_{\mathrm{SR}}}}\right)\\ &\times\sum_{t=0}^{N-1}\sum_{n=0}^{Km_2-1}\sum_{k=0}^{t(m_{\mathrm{RD}_n}-1)}\frac{1}{k!}\binom{N-1}{t}\frac{N(-1)^t b_k^t}{\Gamma(m_{\mathrm{RD}_n})^{N-1}}\left(\frac{m_{\mathrm{RD}_n}}{\Omega_{\mathrm{RD}_n}}\right)^{m_{\mathrm{RD}_n}+t}\left(\frac{m_2\Delta_2}{\Omega_{\mathrm{PR}}}\right)^n\\ &\times 2\left(\frac{m_2\Omega_{\mathrm{RD}_n}\Delta_2}{m_{\mathrm{RD}_n}(t+1)\Omega_{\mathrm{PR}}}\right)^{\frac{k+m_{\mathrm{RD}_n}-n}{2}}\mathcal{K}_{k+m_{\mathrm{RD}_n}-n}\left(2\sqrt{\frac{m_2m_{\mathrm{RD}_n}(t+1)\Delta_2}{\Omega_{\mathrm{PS}}\Omega_{\mathrm{SR}}}}\right).\end{aligned} \tag{25}$$

where $\Delta_1 = \frac{\theta_n^*\sigma_{\mathrm{R}}^2}{\phi\left(a_m-\theta_n^*\sum_{i=m+1}^{N}a_i+\delta_1\sum_{j=1}^{n-1}a_j\right)}$, $\Delta_2 = \frac{\theta_n^*\sigma_{\mathrm{D}_m}^2}{\phi\left(a_m-\theta_n^*\sum_{i=m+1}^{M}a_i+\delta_2\sum_{j=1}^{n-1}a_j\right)}$, and $\phi = \frac{2\alpha\eta P_{\mathrm{PB}}}{1-\alpha}$.

### *3.3. Optimal time switching ratio for maximizing throughput*

The objective of this subsection is to maximize the instantaneous throughput of the proposed PB-assisted EH-NOMA multi-user relaying system. We realize that there is an optimal time switching ratio $\alpha^*$ which provides the highest instantaneous throughput. After the energy harvesting duration $\alpha T$, the remaining time duration $(1-\alpha)T$ is used for the communication between S and $\mathrm{D}_n$. Thus, we only need to determine $\alpha^*$ for one of users. Without loss of generality, we consider the time switching ratio of the last user $\mathrm{D}_N$.

Specifically, the end-to-end instantaneous throughput of $\mathrm{D}_N$ can be computed as

$$R_{x_N}(\alpha)=\frac{(1-\alpha)}{2}\log_2\left(1+\min\left\{\frac{\alpha u}{1-\alpha},\frac{\alpha v}{1-\alpha}\right\}\right), \tag{26}$$

where $u = 2\eta P_B a_N||\mathbf{f_1}||^2|h_1|^2$ and $v = 2\eta P_B a_N||\mathbf{f_2}||^2|g_N|^2$.

The optimal value of $\alpha$ which maximizes the system throughput can be obtained by solving the following optimization problem

$$\begin{aligned}&\alpha^* = \arg\max_{\alpha} R_{x_N}(\alpha),\\ &\text{subject to } 0<\alpha<1.\end{aligned} \tag{27}$$

Taking the partial derivative of (26) with respect to $\alpha$ and letting $\partial R_{x_N}(\alpha)/\partial\alpha = 0$, we have

$$c_0+\frac{c_0\alpha}{1-\alpha} = \left(1+\frac{c_0\alpha}{1-\alpha}\right)\ln\left(1+\frac{c_0\alpha}{1-\alpha}\right). \tag{28}$$

where $c_0 \in \{u, v\}$.

Let $z = 1 + c_0\alpha/(1-\alpha)$, we have

$$c_0 - 1 + z = z\ln z. \tag{29}$$

After some algebraic manipulations, (29) becomes

$$\frac{c_0-1}{e} = \exp\left(\ln\frac{z}{e}\right)\ln\left(\frac{z}{e}\right). \tag{30}$$

Using the definition of Lambert $W(z)$ function [30], $z$ is given by

$$z = e^{W\left(\frac{c_0-1}{e}\right)+1}. \tag{31}$$

Finally, solving (29) with respect to $\alpha$, we obtain the optimal value of $\alpha$ as

$$\alpha^* = \frac{e^{W(\frac{c_0-1}{e})+1} - 1}{c_0 + e^{W(\frac{c_0-1}{e})+1} - 1}, \tag{32}$$

where $W(z)$ is the Lambert $W$ function, satisfying $W(z)\exp(W(z)) = z$.

### *3.4. Comparison of the sum rates of NOMA and OMA relaying systems*

In this subsection, we compare the sum rate of NOMA and OMA systems with three users. We assign a bandwidth $\beta$ Hz for $D_1$ and the remaining bandwidth $(1-\beta)$ Hz for $D_2$ and $D_3$, where $0 < \beta < 1$.

For OMA relaying system, orthogonal frequency division multiple access (OFDMA) is used [31]. From [31, Eq. (7.4)], we can extend the sum rate of OMA relaying system with three users as

$$\mathrm{C_{OMA}} = \frac{1-\alpha}{2}\beta \log_2\left(1+\gamma_{\mathrm{SRD_1}}\right) + \frac{(1-\alpha)(1-\beta)}{4}\log_2\left(1+\gamma_{\mathrm{SRD_2}}\right) + \frac{(1-\alpha)(1-\beta)}{4}\log_2\left(1+\gamma_{\mathrm{SRD_3}}\right), \tag{33}$$

where $\gamma_{\mathrm{SRD_n}}, n \in \{1,2,3\}$, is the end-to-end instantaneous SNR of $\mathrm{S-R-D}_n$ path. Specifically,

$$\gamma_{\mathrm{SRD_1}} = \min\left(\frac{P_{\mathrm{S}}^{\mathrm{OMA}}|h_1|^2}{\beta}, \frac{P_{\mathrm{R}}^{\mathrm{OMA}}|g_1|^2}{\beta}\right), \tag{34}$$

$$\gamma_{\mathrm{SRD_2}} = \min\left(\frac{2P_{\mathrm{S}}^{\mathrm{OMA}}|h_1|^2}{1-\beta}, \frac{2P_{\mathrm{R}}^{\mathrm{OMA}}|g_2|^2}{1-\beta}\right), \tag{35}$$

$$\gamma_{\mathrm{SRD_3}} = \min\left(\frac{2P_{\mathrm{S}}^{\mathrm{OMA}}|h_1|^2}{1-\beta}, \frac{2P_{\mathrm{R}}^{\mathrm{OMA}}|g_3|^2}{1-\beta}\right). \tag{36}$$

In contrast, according to the NOMA theory, the sum rate of NOMA relaying system is the summation of the capacity of all users, i.e.,

$$\mathrm{C_{NOMA}} = \frac{1-\alpha}{2}\log_2\left(1+\Psi_{\mathrm{SRD_1}}\right) + \frac{(1-\alpha)}{2}\log_2\left(1+\Psi_{\mathrm{SRD_2}}\right) + \frac{(1-\alpha)}{2}\log_2\left(1+\Psi_{\mathrm{SRD_3}}\right), \tag{37}$$

where $\Psi_{\mathrm{SRD}n}$, $n \in \{1,2,3\}$, are given as follows.

$$\Psi_{\mathrm{SRD_1}} = \min\left(\frac{a_1 P_{\mathrm{S}}|h_1|^2}{(a_2+a_3)P_{\mathrm{S}}|h_1|^2 + \sigma_{\mathrm{R}}^2}, \frac{a_1 P_{\mathrm{R}}|g_1|^2}{(a_2+a_3)P_{\mathrm{R}}|g_1|^2 + \sigma_{\mathrm{D_1}}^2}\right), \tag{38}$$

$$\Psi_{\mathrm{SRD_2}} = \min\left(\frac{a_2 P_{\mathrm{S}}|h_1|^2}{(\delta_1 a_1+a_3)P_{\mathrm{S}}|h_1|^2 + \sigma_{\mathrm{R}}^2}, \frac{a_2 P_{\mathrm{R}}|g_2|^2}{(\delta_2 a_1+a_3)P_{\mathrm{R}}|g_2|^2 + \sigma_{\mathrm{D_2}}^2}\right), \tag{39}$$

$$\Psi_{\mathrm{SRD_3}} = \min\left(\frac{a_3 P_{\mathrm{S}}|h_1|^2}{\delta_1(a_1+a_2)P_{\mathrm{S}}|h_1|^2 + \sigma_{\mathrm{R}}^2}, \frac{a_3 P_{\mathrm{R}}|g_3|^2}{\delta_2(a_1+a_2)P_{\mathrm{S}}|g_3|^2 + \sigma_{\mathrm{D_3}}^2}\right). \tag{40}$$

It should be noted that when $\delta_1 = \delta_2 = 0$, the SIC is perfect. Otherwise, SIC is imperfect.

### *3.5. The case of nonlinear EH model*

In practice, the output power of the EH circuit is only proportional to the harvested input power up to certain threshold $P_{\mathrm{th}}$. As the input power exceeds this threshold, the output power remains unchanged. This nonlinear EH model reflects the joint effects of the light sensitivity limit and the current leakage of the EH circuit. As the

result of this nonlinear characteristic, the transmission power of S and R in the case of nonlinear EH model can be obtained by extending (5) and (6), i.e.,

$$P_{\mathrm{S}} = \frac{2\alpha\eta}{1-\alpha}\min(P_{\mathrm{PB}}\|\mathbf{f}_1\|^2, P_{\mathrm{th}}) = \begin{cases} \frac{2\alpha\eta}{1-\alpha}P_{\mathrm{PB}}\|\mathbf{f}_1\|^2, & P_{\mathrm{PB}}\|\mathbf{f}_1\|^2 \le P_{\mathrm{th}}, \\ \frac{2\alpha\eta}{1-\alpha}P_{\mathrm{th}}, & P_{\mathrm{PB}}\|\mathbf{f}_1\|^2 > P_{\mathrm{th}}, \end{cases} \tag{41}$$

$$P_{\mathrm{R}} = \frac{2\alpha\eta}{1-\alpha}\min(P_{\mathrm{PB}}\|\mathbf{f}_2\|^2, P_{\mathrm{th}}) = \begin{cases} \frac{2\alpha\eta}{1-\alpha}P_{\mathrm{PB}}\|\mathbf{f}_2\|^2, & P_{\mathrm{PB}}\|\mathbf{f}_2\|^2 \le P_{\mathrm{th}}, \\ \frac{2\alpha\eta}{1-\alpha}P_{\mathrm{th}}, & P_{\mathrm{PB}}\|\mathbf{f}_2\|^2 > P_{\mathrm{th}}. \end{cases} \tag{42}$$

Consequently, in the case of non-linear EH model, the SINR of S − R link becomes

$$\Gamma_1^n = \begin{cases} \dfrac{a_n\kappa P_{\mathrm{PB}}\|\mathbf{f_1}\|^2|h_1|^2}{\sum_{i=n+1}^{N} a_i\kappa P_{\mathrm{PB}}||\mathbf{f_1}||^2|h_1|^2 + \sigma_{\mathrm{R}}^2} & \text{if } P_{\mathrm{PB}}\|\mathbf{f}_1\|^2 \le P_{\mathrm{th}}, \quad (43a) \\ \dfrac{a_n\kappa P_{\mathrm{th}}|h_1|^2}{\sum_{i=n+1}^{N} a_i\kappa P_{\mathrm{th}}|h_1|^2 + \sigma_{\mathrm{R}}^2} & \text{if } P_{\mathrm{PB}}\|\mathbf{f}_1\|^2 > P_{\mathrm{th}}, \quad (43b) \end{cases}$$

and the SINR of $\mathrm{D}_n$ when the signal of $j$th user, $j < n$, exists is given by

$$\Gamma_2^{j\to n} = \begin{cases} \dfrac{a_j\kappa P_{\mathrm{PB}}||\mathbf{f_2}||^2|g_n|^2}{\sum_{i=j+1}^{N} a_i\kappa P_{\mathrm{PB}}||\mathbf{f_2}||^2|g_n|^2 + \sigma_{\mathrm{D}_n}^2} & \text{if } P_{\mathrm{PB}}\|\mathbf{f}_2\|^2 \le P_{\mathrm{th}}, \quad (44a) \\ \dfrac{a_j\kappa P_{\mathrm{th}}|g_n|^2}{\sum_{i=j+1}^{N} a_i\kappa P_{\mathrm{th}}|g_n|^2 + \sigma_{\mathrm{D}_n}^2} & \text{if } P_{\mathrm{PB}}\|\mathbf{f}_2\|^2 > P_{\mathrm{th}}, \quad (44b) \end{cases}$$

where $\kappa = \frac{2\alpha\eta}{1-\alpha}$.

From these SINR expressions and using similar calculations as in previous subsections, we can get the outage probability and ergodic capacity of the considered PB-assisted EH-NOMA multi-user relaying system in the case of linear EH model.

## 4. Numerical results

In this section, we provide the numerical results to investigate the performance in terms of the outage probability (OP), throughput, and sum rate of the considered PB-assisted EH-NOMA multi-user relaying system. We also determine the optimal time switching ratio which maximizes the system throughput. In addition, we compare the sum rates of NOMA and OMA relaying systems. Since the complexity and performance degradation of each user in NOMA systems is proportional to the number of users $N$ [32], we choose $N = 3$. The power allocation coefficient of $\mathrm{D}_n$ is $a_n = (N - n + 1)/\mu$, where $\mu$ is chosen so that $\sum_{n=1}^{N}\sqrt{a_n} = 1$. The average SNR is defined as $P_{\mathrm{PB}}/\sigma^2$. Unless otherwise stated, the system parameters used in the following performance evaluation are summarized in Table 2.

Fig. 3 shows the OP versus the average SNR in dB for different fading degrees. We consider two cases of $m$ for all Nakagami-$m$ fading channels, i.e. case I: $m = 1$ and case II: $m = 2$. As can be seen in Fig. 3, the OP decreases as $m$ increases. However, the OP of $\mathrm{D}_3$ is the best although the power allocation for it is lowest because $\mathrm{D}_3$ is

Table 2: The system parameters used in the performance evaluation.

| **System parameter** | **Value** |
|---|---|
| The number of users | $N = 3$ |
| The number of antennas of PB | $K = 1, 2, 3$ |
| Power allocation coefficients | $a_1 = 0.6, a_2 = 0.2, a_3 = 0.1$ |
| The average channel gain | $\Omega_{\text{PB-S}} = \Omega_{\text{PB-R}} = \Omega_{\text{SR}} = \Omega_{RD_1} = 2$, $\Omega_{RD_2} = 3$, and $\Omega_{RD_3} = 4$ |
| The threshold data rate | $r_1 = 1.5$ b/s/Hz, $r_2 = 1$b/s/Hz, and $r_3 = 0.5$b/s/Hz |
| Time switching ratio | $\alpha = 0.2$ |
| Energy conversion efficiency | $\eta = 0.85$ |
| The levels of residual interference at R and $\text{D}_n$ | $\delta_1 = 0.02, \delta_2 = 0.04$ |
| The fading severity of PB$-S$, PB$-R$, $\text{S} - \text{R}$, and $\text{R} - \text{D}_n$ channels | $m = 1, 2$ |
| The transmission block period | $T = 1$ sec |

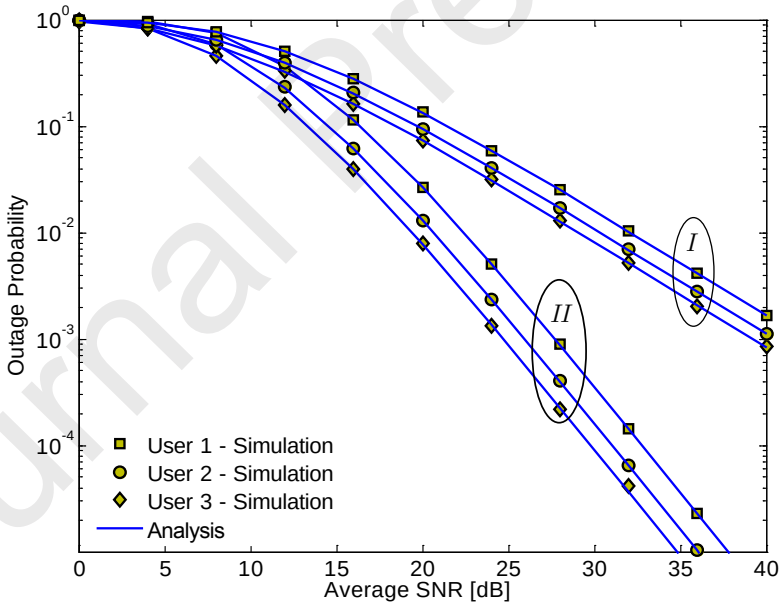


Figure 3: The OPs of $\text{D}_1$, $\text{D}_2$, and $\text{D}_3$ versus the average SNR for different fading degrees.

closest to R[2]. We can also see that the system diversity of case II is larger than that of case I. Specifically, the diversity order of case I equals to one while the diversity order of the case II equals to two.

From now, we will use $m = 2$ for all Nakagami-$m$ fading channels. Fig. 4 plots the OPs of $\text{D}_1$, $\text{D}_2$, and $\text{D}_3$

[2]The decay of the magnitude power signal is proportional to the squared distance in multipath rays fading [28, pp.33].

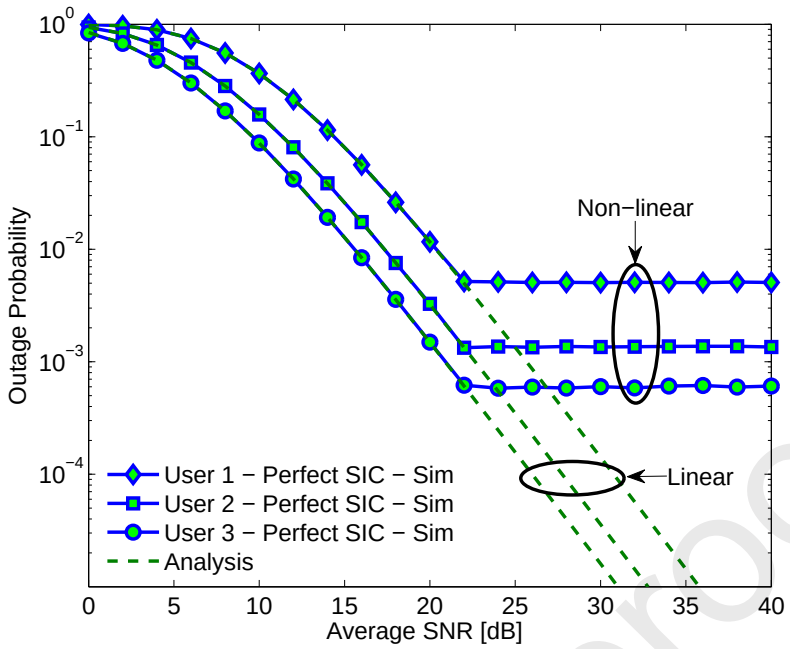


Figure 4: Outage probability of each user versus the average SNR for linear and non-linear EH models.

versus the average SNR in dB for linear and nonlinear EH models. The SIC is perfect. Other parameters are as follows: $K = 2$, $P_{\text{th}} = 25$ dB. From Fig. 4, we can see that up to a specific average SNR (average SNR $\leq 22$ dB in this scenario), the OPs of all users in the case of nonlinear EH model are the same as those in the case of linear EH model. However, as the SNR gets higher, the OPs of all users in the case of linear EH model continues to decrease while OPs of all users in the case of nonlinear EH model keeps unchanged. It is because of the nonlinear relationship of the output power of the EH circuit and the harvested input power as mentioned in Subsection 3.5.

Fig. 5 presents the OPs of $D_1$, $D_2$, and $D_3$ versus the average SNR in dB for both perfect SIC and imperfect SIC. The coefficients of imperfect SIC at R is $\delta_1 = 0.02$ and at each user is $\delta_{2,n} = 0.04$. As observed in Fig. 5, the OPs of $D_2$ and $D_3$ in the case of imperfect SIC are always higher than those in the case of perfect SIC. Meanwhile, the OPs of $D_1$ in both cases of imperfect SIC and perfect SIC are similar and they are the highest compared with the OPs of other users because SIC is not applied at $D_1$ and the distance from R to $D_1$ is farthest. In contrast, the OP of $D_3$ in the case of perfect SIC is lowest because $D_3$ is closest to R, thus the channel gain of $R - D_3$ channel is largest. On the other hand, the OP of $D_3$ is worse than $D_2$ in the case of imperfect SIC due to the existence of SIC error (or can be called as error propagation [33, pp. 242]).

Fig. 6 demonstrates the impact of time switching ratio $\alpha$ on the OP of $D_2$ as its values range from 0 to 1. The SNR is fixed at 15 dB. We can see that there exists an optimal value of $\alpha$, which minimizes OP of $D_2$. Moreover, for different numbers of antennas of PB, different minimal OPs of $D_2$ can be achieved. Specifically, higher number of antennas results in lower OP. Another important observation is that the value of $\alpha$ which minimizes the OP of $D_2$ is approximately 0.25 regardless of the number of antennas of PB.

Fig. 7 plots the OPs of $D_1$, $D_2$, and $D_3$ versus the coefficient of imperfect SIC. It is assumed that the coefficients of imperfect SIC at R and $D_n$ are similar, i.e. $\delta_1 = \delta_{2,n} = \delta$, with $0 \leq \delta \leq 1$. From Fig. 7, we can see that increasing the coefficient of imperfect SIC leads to an increase in the OPs of $D_2$ and $D_3$ but not the OP of $D_1$

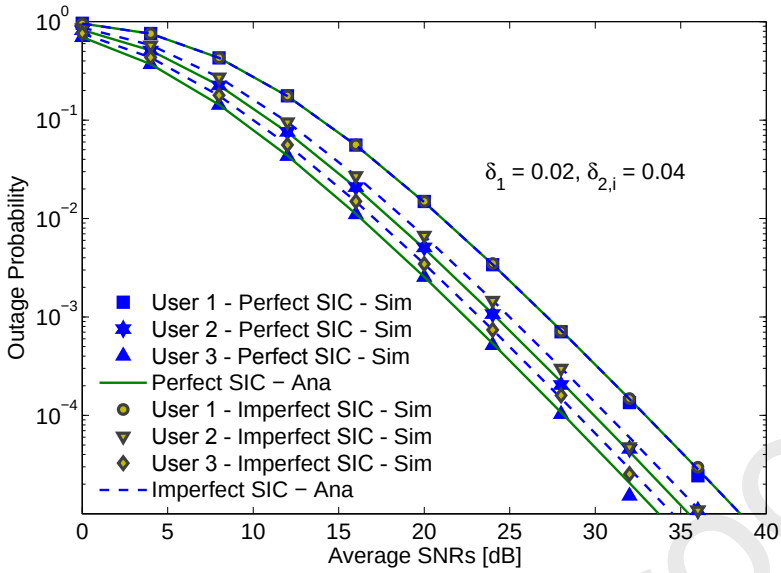


Figure 5: The OPs of $D_1$, $D_2$, and $D_3$ versus the average SNR for perfect and imperfect SIC.

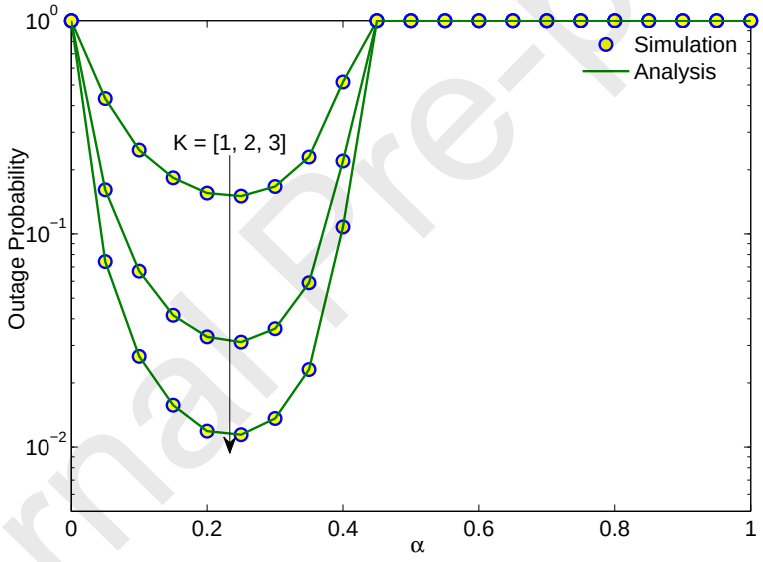


Figure 6: The OP of $D_2$ versus the time switching ratio $\alpha$ for different numbers of antennas of PB. The average SNR = 15 dB.

because SIC is only applied at $D_2$ and $D_3$. Moreover, we can see that the OP of $D_3$ is higher than $D_2$, indicating that effect of imperfect SIC on $D_3$ is more serious than $D_2$. It is obvious because SIC must be applied two times at $D_3$ to remove the signals of $D_1$ and $D_2$, while only one-time SIC is needed at $D_2$ to remove the signal of $D_1$. In other words, since the residual power after SIC at a specific user acts as the linear co-interference for latter users, the performance degradation of each users scales up with the number of users. Therefore, dividing all users into several clusters may help to increase the performance of each user.

Fig. 8 shows the throughput versus the time switching ratio $\alpha$ for perfect SIC and different numbers of antennas of PB. We can see from Fig 8 that, increasing the number of antennas results in the decrease in the optimal value of $\alpha$ and the increase in the system throughput. This feature happens because the improvement in the channel

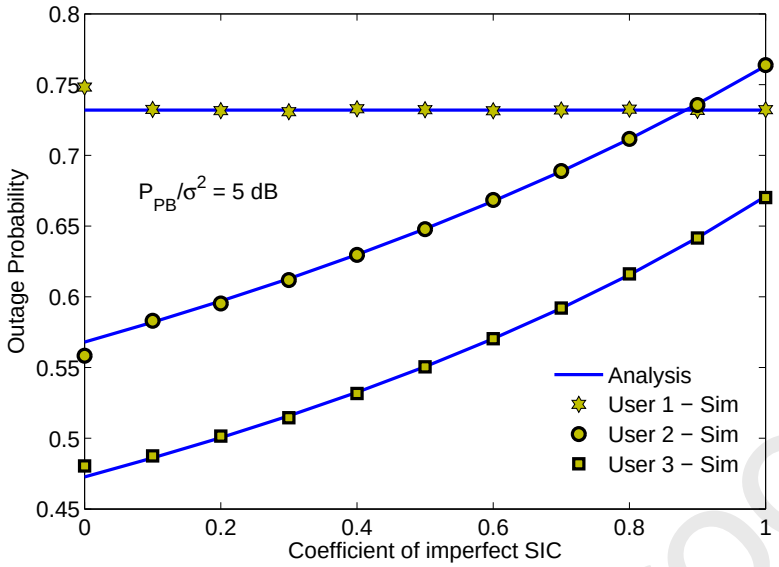


Figure 7: The OPs of $D_1$, $D_2$, and $D_3$ versus the coefficient of imperfect SIC. The average SNR = 5 dB.

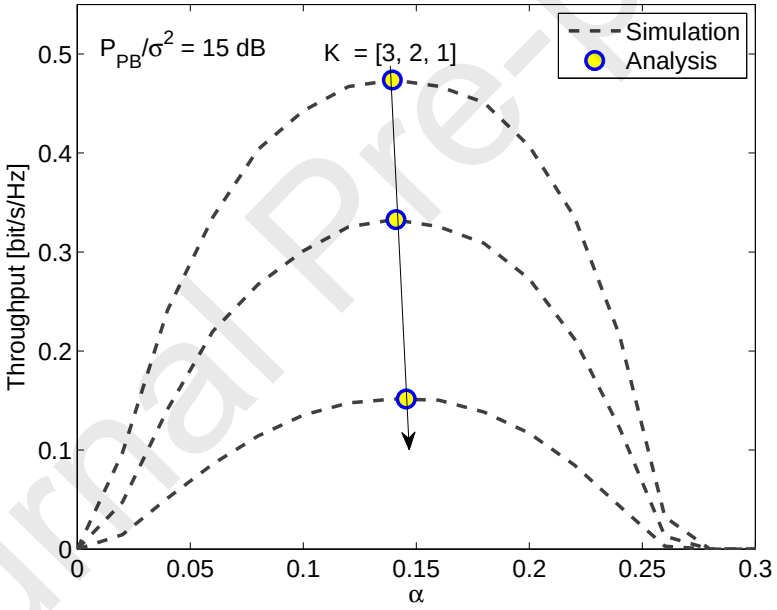


Figure 8: Throughput versus the time switching ratio $\alpha$ for different numbers of antennas of PB. The average SNR = 15 dB.

gains of PB − S and PB − R channels increases the amount of harvested energy. Thus, based on Fig 8, we can select a suitable period during which the PB transmits the energy to S and R so that the system throughput is maximized. For example, for $K = 3$ and $K = 1$, the optimal time switching ratio can be set at $\alpha = 0.12T$ and $\alpha = 0.14T$, respectively.

Fig. 9 depicts the simulation results of the sum rates of NOMA and OMA relaying systems versus the average SNR in dB. The number of antennas of PB is $K = 2$. The coefficients of imperfect SIC at R and $D_n$ are similar, i.e. $\delta_1 = \delta_{2,n} = \delta$. We study four cases of $\delta$, i.e. $\delta = [0.01, 0.02, 0.03, 0.04]$. It is noticed that when $\delta = 0$, SIC is perfect. As can be seen in Fig. 9, the sum rate of NOMA relaying system in the case of perfect SIC is always better than

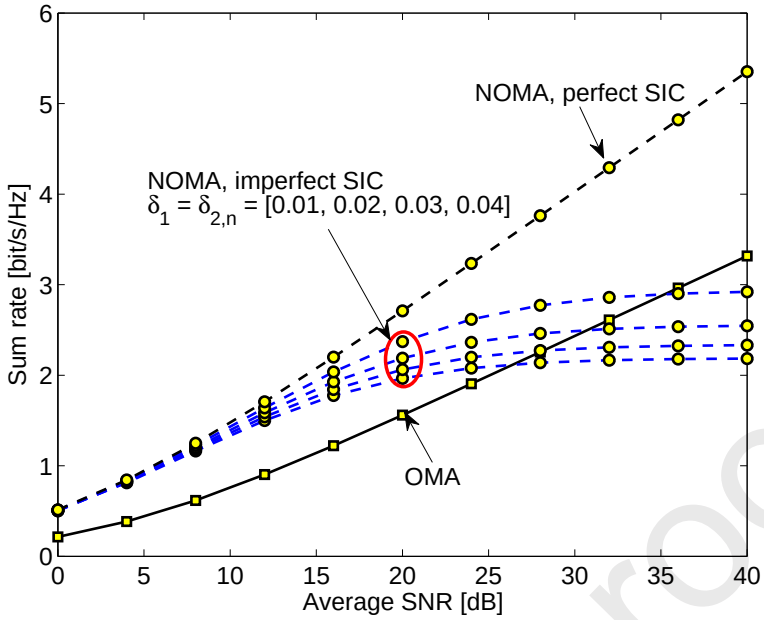


Figure 9: Comparison of the sum rate of NOMA and OMA relaying systems versus the average SNR in dB. The number of antennas of PB is $K = 2$.

that of OMA relaying system. It is because a whole bandwidth is used for each user in NOMA relaying system, while this bandwidth must be shared among three users in OMA relaying system. Thus, the spectrum utilization of NOMA relaying system is higher than OMA relaying system. We can also observe in Fig. 9 that, the achievable sum rate of NOMA relaying system in the case of imperfect SIC depends on $\delta$. Specifically, for the same average SNR, the sum rate is lower as $\delta$ increases. Moreover, the sum rate is saturated in the high SNR regime because of the increased interference caused by the imperfect SIC process.

## 5. Conclusions

In this paper, we have analyzed a PB-assisted EH-NOMA multi-user relaying system for the cases of perfect and imperfect SIC over Nakagami-$m$ fading channels. Particularly, we gave detailed derivations of the exact closed-form expression of the OP for both perfect and imperfect SIC. Then, we calculated the optimal time switching ratio which maximizes the system throughput. We also compared the sum rates of the proposed NOMA relaying system with that of the OMA relaying system. Some important conclusions can be summarized as follows:

- The fading severity of wireless channels remarkably affects the OP and diversity. In particular, less fading severity (corresponding to higher $m$) greatly reduces the OPs of all users, especially the user locates near the relay, and increases the system diversity.

- Compared with the OPs of all users in the case of linear EH model, the OPs of all users in the case of nonlinear EH model is similar when the SNR less than a specific value but keeps unchanged as the SNR continues to increase.

- Applying SIC helps to reduce the OP. Specifically, the higher SIC capability of user is, the lower OP can be achieved. Furthermore, due to the SIC error, users which are far from the relay suffer from higher OP.
- There exists an optimal value of time switching ratio on the OP of a user. Moreover, increasing the number of antennas of PB results in lower OP of all users and higher system throughput. Therefore, we can select a suitable period during which the PB transmits the energy so that the system throughput can be maximized.
- The sum rate of the proposed NOMA relaying system directly depends on the SIC quality. Meanwhile, it is always better than that of the OMA relaying system in low and moderate SNR regimes.

In our future work, we will extend to a system with multiple relays operating under the imperfect CSI.

**Acknowledgment**

The authors would like to thanks Dr. Tran Trung Duy for his valuable comments which help to improve the quality of this paper.

**Appendix**

This appendix gives the detailed derivations of (18) and (25).

From the instantaneous SINR given in (12), we begin with the following probability

$$\begin{aligned}\mathcal{O}_1 &= \Pr(\Gamma_1^n > \theta_n^*) \\ &= \Pr\left(||\mathbf{f_1}||^2|h_1|^2 > \frac{\theta_n^*}{\phi(a_n - \sum_{i=n+1}^{N} a_i\theta_n^*)}\right) \\ &= \int_0^\infty \left[1 - F_{||\mathbf{f_1}||^2}\left(\frac{\chi_1}{y}\right)\right] f_Y(y)dy. \end{aligned} \tag{45}$$

Plugging (8) and (9) into (45), we have

$$\begin{aligned}\mathcal{O}_1 = &\sum_{\nu=0}^{Km_1-1} \frac{1}{\nu!\Gamma(m_{\mathrm{SR}})}\Big(\frac{m_1\chi_1}{\Omega_{\mathrm{PS}}}\Big)^n\Big(\frac{m_{\mathrm{SR}}}{\Omega_{\mathrm{SR}}}\Big)^{m_{\mathrm{SR}}} \\ &\times \int_0^\infty y^{m_{\mathrm{SR}}-\nu-1}\exp\Big(-\frac{m_1\chi_1}{y\Omega_{\mathrm{PS}}} - \frac{m_{\mathrm{SR}}y}{\Omega_{\mathrm{SR}}}\Big)dy. \end{aligned} \tag{46}$$

From [21, Eq. (3.471.9)] and after some manipulations, we obtain the first term $\mathcal{O}_1$ of (17) as

$$\begin{aligned}\mathcal{O}_1 = &\sum_{\nu=0}^{Km_1-1} \frac{2}{\nu!\Gamma(m_{\mathrm{SR}})}\left(\frac{m_1\chi_1}{\Omega_{\mathrm{PS}}}\right)^\nu\left(\frac{m_1\Omega_{\mathrm{SR}}\chi_1}{m_{\mathrm{SR}}\Omega_{\mathrm{PS}}}\right)^{\frac{m_{\mathrm{SR}}-\nu}{2}} \\ &\times\left(\frac{m_{\mathrm{SR}}}{\Omega_{\mathrm{SR}}}\right)^{m_{\mathrm{SR}}}\mathcal{K}_{m_{\mathrm{SR}}-\nu}\left(2\sqrt{\frac{m_1m_2\chi_1}{\Omega_{\mathrm{PS}}\Omega_{\mathrm{SR}}}}\right). \end{aligned} \tag{47}$$

To obtain the second term $\mathcal{O}_2$ of (17), we start from the instantaneous SINR given in (14). Particularly,

$$\begin{aligned}\mathcal{O}_2 &= \Pr(\Gamma_2^{j\to n} > \theta_n^*) \\ &= \Pr\left(||\mathbf{f_2}||^2|g_n|^2 > \frac{\theta_n^*}{\phi(a_n - \sum_{i=j+1}^{N} a_i\theta_m^*)}\right) \\ &= \int_0^\infty \left[1 - F_{||\mathbf{f_2}||^2}\left(\frac{\chi_2}{x}\right)\right] f_{|g_n|^2}(x)dx, \end{aligned} \tag{48}$$

where $F_{||\mathbf{f_2}||^2}\left(\frac{\chi_2}{x}\right)$ is given in (9).

For $f_{|g_n|^2}(x)$, it can be represented as the PDF of the ordered statistic variables $X_i$ [34, Eq.(7.14)], i.e.,

$$f_{|g_n|^2}(x) = N f_{X_i}(x)[F_{X_i}(x)]^{N-1}, \tag{49}$$

where

$$f_{X_i}(x) = \left(\frac{m_{\mathrm{RD}_n}}{\Omega_{\mathrm{RD}_n}}\right)^{m_{\mathrm{RD}_n}} \frac{x^{m_{\mathrm{RD}_n}-1}}{\Gamma(m_{\mathrm{RD}_n})} \exp\left(-\frac{m_{\mathrm{RD}_n}x}{\Omega_{\mathrm{RD}_n}}\right), \tag{50}$$

and

$$F_{X_i}(x) = 1 - \exp\left(-\frac{m_{\mathrm{RD}_n}x}{\Omega_{\mathrm{RD}_n}}\right) \sum_{k=1}^{m_{\mathrm{RD}_n}-1} \frac{1}{k!}\left(\frac{m_{\mathrm{RD}_n}x}{\Omega_{\mathrm{RD}_n}}\right)^k, \tag{51}$$

Substituting (50) and (51) into (49), we have

$$\begin{aligned} f_{|g_n|^2}(x) = &\sum_{t=0}^{N-1} \binom{N-1}{t} \frac{N x^{m_{\mathrm{RD}_n}-1}(-1)^t}{\Gamma(m_{\mathrm{RD}_n})^{N-1}} \\ &\times \left(\frac{m_{\mathrm{RD}_n}}{\Omega_{\mathrm{RD}_n}}\right)^{m_{\mathrm{RD}_n}} \exp\left(-\frac{m_{\mathrm{RD}_n}(t+1)x}{\Omega_{\mathrm{RD}_n}}\right) \\ &\times \left[\sum_{k=0}^{m_{\mathrm{RD}_n}-1} \frac{1}{k!}\left(\frac{m_{\mathrm{RD}_n}x}{\Omega_{\mathrm{RD}_n}}\right)^k\right]^t. \end{aligned} \tag{52}$$

The inner summation $\left[\sum_{k=0}^{m_{\mathrm{RD}_n}-1} \frac{1}{k!}\left(\frac{m_{\mathrm{RD}_n}x}{\Omega_i}\right)^k\right]^t$ in (52) is a polynomial of $(m_{\mathrm{RD}_n}-1)$th degree with respect to the variable $z = \frac{m_{\mathrm{RD}_n}x}{\Omega_{\mathrm{RD}_n}}$. The $t$th power of this polynomial is a polynomial of $t(m_{\mathrm{RD}_n}-1)$th degree. Thanks to [21, Eq. (0.314)], it can be reduced to

$$\left[\sum_{k=0}^{m_{\mathrm{RD}_n}-1} \frac{1}{k!}\left(\frac{m_{\mathrm{RD}_n}x}{\Omega_{\mathrm{RD}_n}}\right)^k\right]^t = \sum_{k=0}^{t(m_{\mathrm{RD}_n}-1)} (b_k^t z^k), \tag{53}$$

where $b_k^t$ is presented in (19a), (19b) and (19c).

Next, we combine (9), (52), and (48) to obtain

$$\begin{aligned}\mathcal{O}_2 = &\sum_{t=0}^{N-1}\sum_{n=0}^{Km_2-1} \frac{1}{k!}\binom{N-1}{t}\left(\frac{m_2\chi_2}{\Omega_{PR}}\right)^n \times \sum_{k=0}^{t(m_{\mathrm{RD}_n}-1)} \frac{N(-1)^t b_k^t}{\Gamma(m_{\mathrm{RD}_n})^{N-1}}\left(\frac{m_{\mathrm{RD}_n}}{\Omega_{\mathrm{RD}_n}}\right)^{m_{\mathrm{RD}_n}+k} \\ &\times \int_0^\infty x^{k+m_{\mathrm{RD}_n}-n-1} \exp\left(-\frac{m_2\chi_2}{\Omega_{\mathrm{PR}}x} - \frac{m_{\mathrm{RD}_n}(t+1)x}{\Omega_{\mathrm{RD}_n}}\right) dx. \end{aligned} \tag{54}$$

Then, using [21, Eq. (3.471.9)] and after some manipulations, we obtain the second term $\mathcal{O}_2$ of (17) as

$$\mathcal{O}_2 = \sum_{t=0}^{N-1} \sum_{n=0}^{Km_2-1} \sum_{k=0}^{t(m_{\mathrm{RD}_n}-1)} \frac{1}{k!}\binom{N-1}{t} \left(\frac{m_{\mathrm{RD}_n}}{\Omega_{\mathrm{RD}_n}}\right)^{m_{\mathrm{RD}_n}+k} \times \frac{N(-1)^t b_k^t}{\Gamma(m_{\mathrm{RD}_n})^{N-1}} \left(\frac{m_2\chi_2}{\Omega_{\mathrm{PR}}}\right)^n \times 2\left(\frac{m_2\Omega_{\mathrm{RD}_n}\chi_2}{m_{\mathrm{RD}_n}(t+1)\Omega_{\mathrm{PR}}}\right)^{\frac{k+m_{\mathrm{RD}_n}-n}{2}} \times \mathcal{K}_{k+m_{\mathrm{RD}_n}-n}\left(2\sqrt{\frac{m_2 m_{\mathrm{RD}_n}(t+1)\chi_2}{\Omega_{\mathrm{PS}}\Omega_{\mathrm{SR}}}}\right). \quad (55)$$

Finally, we combine (47) and (55) to obtain the closed-form expression of the OP in the case of perfect SIC as in (18).

Similarly, we can derive the closed-form expression of the OP in the case of imperfect SIC as in (25) by using the conditional probability as described above.

## References


[1] Y. Liu, Z. Qin, M. Elkashlan, Z. Ding, A. Nallanathan, L. Hanzo, Nonorthogonal multiple access for 5g and beyond, Proceedings of the IEEE 105 (12) (2017) 2347–2381.

[2] Y. Liu, Z. Qin, M. Elkashlan, A. Nallanathan, J. A. McCann, Non-orthogonal multiple access in large-scale heterogeneous networks, IEEE Journal on Selected Areas in Communications 35 (12) (2017) 2667–2680.

[3] T. Lv, Y. Ma, J. Zeng, P. T. Mathiopoulos, Millimeter-wave noma transmission in cellular m2m communications for internet of things, IEEE Internet of Things Journal 5 (3) (2018) 2370–2382.

[4] T. D. P. Perera, D. N. K. Jayakody, S. K. Sharma, S. Chatzinotas, J. Li, Simultaneous wireless information and power transfer (swipt): Recent advances and future challenges, IEEE Communications Surveys & Tutorials 20 (1) (2017) 264–302.

[5] R. Sun, Y. Wang, X. Wang, Y. Zhang, Transceiver design for cooperative non-orthogonal multiple access systems with wireless energy transfer, IET Communications 10 (15) (2016) 1947–1955.

[6] W. H. . J. G. . J. Men, Performance analysis for noma energy harvesting relaying networks with transmit antenna selection and maximal-ratio combining over nakagami-m fading, IET Communications 10 (18) (2016) 2687–2693.

[7] W. Hao, Z. Chu, F. Zhou, S. Yang, G. Sun, K.-K. Wong, Green communication for NOMA-based CRAN, IEEE Internet of things journal 6 (1) (2018) 666–678.

[8] Y. Liu, Z. Ding, M. Elkashlan, H. V. Poor, Cooperative non-orthogonal multiple access with simultaneous wireless information and power transfer, IEEE Journal on Selected Areas in Communications 34 (4) (2016) 938–953.

[9] T. M. Hoang, N. T. Tan, N. H. Hoang, P. T. Hiep, Performance analysis of decode-and-forward partial relay selection in noma systems with rf energy harvesting, Wireless Networks (2018) 1–11.

[10] Z. Yang, Z. Ding, P. Fan, N. Al-Dhahir, The impact of power allocation on cooperative non-orthogonal multiple access networks with swipt, IEEE Transactions on Wireless Communications 16 (7) (2017) 4332–4343.

[11] Y. Liu, L. Wang, S. A. R. Zaidi, M. Elkashlan, T. Q. Duong, Secure d2d communication in large-scale cognitive cellular networks: A wireless power transfer model, IEEE Transactions on Communications 64 (1) (2016) 329–342.

[12] K. H. . V. K. N. Lau, Enabling wireless power transfer in cellular networks: Architecture, modeling and deployment, IEEE Transactions on Wireless Communications 13 (2) (2014) 902–912.

[13] C. Xu, M. Zheng, W. Liang, H. Yu, Y.-C. Liang, Outage performance of underlay multihop cognitive relay networks with energy harvesting, IEEE Communications Letters 20 (6) (2016) 1148–1151.

[14] C. Zhong, X. Chen, Z. Zhang, G. K. Karagiannidis, Wireless-powered communications: Performance analysis and optimization, IEEE Transactions on Communications 63 (12) (2015) 5178–5190.

[15] Y. M. . H. C. . Z. L. . Y. L. . B. Vucetic, Distributed and optimal resource allocation for power beacon-assisted wireless-powered communications, IEEE Transactions on Communications 63 (10) (2015) 3569–3583.

[16] X. Zhang, Y. Wang, F. Zhou, N. Al-Dhahir, X. Deng, Robust resource allocation for MISO cognitive radio networks under two practical non-linear energy harvesting models, IEEE Communications Letters 22 (9) (2018) 1874–1877.

[17] H. Sun, F. Zhou, R. Q. Hu, L. Hanzo, Robust beamforming design in a NOMA cognitive radio network relying on SWIPT, IEEE Journal on Selected Areas in Communications 37 (1) (2018) 142–155.

[18] F. Zhou, Z. Chu, H. Sun, R. Q. Hu, L. Hanzo, Artificial noise aided secure cognitive beamforming for cooperative MISO-NOMA using SWIPT, IEEE Journal on Selected Areas in Communications 36 (4) (2018) 918–931.

[19] M. F. Kader, M. B. Shahab, S. Y. Shin, Exploiting non-orthogonal multiple access in cooperative relay sharing, IEEE Communications Letters 21 (5) (2017) 1159–1162.

[20] L. Lv, J. Chen, Q. Ni, Cooperative non-orthogonal multiple access in cognitive radio, IEEE Communications Letters 20 (10) (2016) 2059–2062.

[21] I. S. Gradshteyn, I. M. Ryzhik, Table of integrals, series, and products.

[22] Q. Zhang, Z. Liang, Q. Li, J. Qin, Buffer-aided non-orthogonal multiple access relaying systems in rayleigh fading channels, IEEE Transactions on Communications 65 (1) (2017) 95–106.

[23] A. A. Nasir, X. Zhou, S. Durrani, R. A. Kennedy, Relaying protocols for wireless energy harvesting and information processing, IEEE Transactions on Wireless Communications 12 (7) (2013) 3622–3636.

[24] P. M. Shankar, Fading and shadowing in wireless systems.

[25] M. Ju, K.-M. Kang, K.-S. Hwang, C. Jeong, Maximum transmission rate of psr/tsr protocols in wireless energy harvesting df-based relay networks, IEEE Journal on Selected Areas in Communications 33 (12) (2015) 2701–2717.

[26] Y. M. . H. C. . Z. L. . Y. L. . B. Vucetic, Distributed and optimal resource allocation for power beacon-assisted wireless-powered communications, IEEE Transactions on Communications 63 (10) (2015) 3569–3583.

[27] T. M. Hoang, V. V. Son, N. C. Dinh, P. T. Hiep, Optimizing duration of energy harvesting for downlink noma full-duplex over nakagami-m fading channel, AEU - International Journal of Electronics and Communications 95 (2018) 199–206.

[28] A. Goldsmith, Wireless communications.

[29] T. Wang, A. Cano, G. B. Giannakis, J. N. Laneman, High-performance cooperative demodulation with decode-and-forward relays, IEEE Transactions on Communications 55 (7) (2007) 1427–1438.

[30] R. M. Corless, G. H. Gonnet, D. E. G. Hare, D. J. Jeffrey, D. E. Knuth, On the lambertw function, Advances in Computational Mathematics 5 (1) (1996) 329–359.

[31] A. Benjebbour, K. Saito, A. Li, Y. Kishiyama, T. Nakamura, Non-orthogonal multiple access (noma): Concept and design, Signal Processing for 5G: Algorithms and Implementations (2016) 143–168.

[32] L. Bariah, S. Muhaidat, A. Al-Dweik, Error probability analysis of non-orthogonal multiple access over nakagami-m fading channels, IEEE Transactions on Communications 67 (2) (2018) 1586–1599.

[33] D. Tse, P. Viswanath, Fundamentals of wireless communication.

[34] A. Papoulis, S. U. Pillai, Probability, random variables and stochastic processes.

**Declaration of interests**

☑The authors declare that they have no known competing financial interests or personal relationships that could have appeared to influence the work reported in this paper.

☐The authors declare the following financial interests/personal relationships which may be considered as potential competing interests: